Applied Catalysis B: Environmental 343 (2024) 123530

Contents lists available at ScienceDirect

Applied Catalysis B: Environmental

journal homepage: www.elsevier.com/locate/apcatb

By-product reduction for the non-thermal plasma removal of toluene using an α-MnO_2/Cordierite honeycomb monolithic catalyst in a honeycomb structure

Qianqian Yan, Jiafan Ji, Yi Chen, Gaosheng Zhao, Bin Jia *, Li Xu, Ping Cheng *

School of Environmental and Chemical Engineering, Shanghai University, Shanghai 200444, China

ARTICLE INFO

Keywords:
α-MnO_2/CHM catalyst
Plasma catalysis
Toluene
Removal of products
Reaction mechanism

ABSTRACT

The practical implementation of non-thermal plasma (NTP) combined with catalysts still faces challenges due to the by-products, such as O_3 and nanoparticles. In this study, α-MnO_2/Cordierite honeycomb monolithic (CHM) catalyst was used to reduce the by-products for NTP degradation of toluene. The by-products analysis shows that using the α-MnO_2/CHM catalyst not only improves the degradation efficiency up to 98% and CO_X selectivity to 50%, but also simultaneously and greatly reduces the release of three types of hazardous by-products, organic components, ozone, and particles. The mechanisms of toluene degradation and by-product formation were investigated through online monitoring which can be summarized in two ways: direct degradation by energetic electrons and reactive radicals in the discharge region, and deep oxidation by active oxygen species on the catalyst surface. This investigation can improve our understanding of VOC degradation by combining monolithic catalysts with plasma, and accelerate the implementation of plasma-catalyzed technology in real-world.

1. Introduction

Volatile organic compounds (VOCs) are the primary precursors of secondary organic aerosols and a significant component of fine particulate matter. These compounds contribute to air pollution issues that pose a serious threat to the environment and human health. The emission and removal of pollutants have attracted extensive attention from researchers and environmentalists. [1–4] Therefore, in order to achieve the goal of reducing VOCs emissions, many countries have enacted increasingly stringent laws and regulations in recent years. These measures aim to control the release of VOCs and have led to the development of various emission reduction technologies. The existing emission reduction technologies are mainly divided into recycling technologies [5–8] and destructive technologies [9–17]. However, it is important to acknowledge that these methods possess certain limitations that restrict their universal applicability in various real-world scenarios. Therefore, the pursuit of further enhancements to effectively address practical issues continues to present challenges. In recent years, there has been significant development in the field of NTP technology. This technology has gained attention due to its ability to effectively remove volatile organic compounds (VOCs) at room temperature and atmospheric pressure, while consuming minimal energy. As a result, it is regarded as a promising solution for reducing VOCs emissions [18]. NTP demonstrates a notable level of energy efficiency due to the fact that the input energy effectively increases the velocities of electrons. As a result, these accelerated electrons collide with molecules, leading to the excitation and ionization of said molecules. This process generates a significant number of active secondary electrons and chemically active species, such as ionic, radical, metastable, and excited species. Importantly, this entire system operates at ambient temperature [19,20]. Subsequently, the aforementioned active species have the capability to undergo oxidation reactions with VOCs, resulting in the production of water (H_2O) and carbon dioxide (CO_2) [21]. NTP technology offers several advantages, including cost-effectiveness, broad applicability, and convenient integration with catalysts [22,23]. However, there is still a need for further improvement in toluene conversion and the reduction of by-product formation, such as O_3 and NO_x [24,25]. These issues can be effectively addressed through the utilization of plasma-catalytic systems [26].

Plasma catalytic systems have been the subject of extensive research aimed at enhancing energy efficiency and, consequently, achieving diverse VOC conversion rates and CO_2 selectivity. For instance, Dong et al. [27] discovered that the plasma-coupled MnO_X/Al_2O_3 catalysts exhibited catalytic activity in the elimination of toluene. This activity

* Corresponding authors.
E-mail addresses: jiabin_bj@shu.edu.cn (B. Jia), Pingcheng@shu.edu.cn (P. Cheng).

https://doi.org/10.1016/j.apcatb.2023.123530
Received 1 September 2023; Received in revised form 27 October 2023; Accepted 14 November 2023
Available online 18 November 2023
0926-3373/© 2023 Elsevier B.V. All rights reserved.

resulted in enhanced mineralization and further oxidation of the intermediate to CO_2, consequently suppressing the formation of NOx. In the past few years, there has been a significant utilization of manganese-based nanocatalysts in the domain of VOCs decomposition [28]. Among the various types of manganese oxides, those with different crystal phases, such as α-, β-, γ-, and ε-, have garnered significant interest due to their remarkable capacity to convert ozone into reactive oxygen species at ambient temperature. Additionally, these manganese oxides are more cost-effective compared to precious metals [29–33]. Compared to other transition metal oxides, catalysts based on Mn exhibit higher activity in the decomposition of VOCs [34] and O_3 [35]. Furthermore, manganese oxide is widely regarded as the preferred catalyst for the oxidation of CO to CO_2, which is a crucial reaction in the process of VOCs [36,37]. Hence, catalysts based on manganese offer several advantages including cost-effectiveness, environmental compatibility, efficient removal of VOCs, oxidation activity, and decomposition activity of O_3 at ambient temperatures. Hong et al. [38] employed a modified α-MnO_2/ZSM-5 catalyst and observed significantly higher toluene conversion and CO_X selectivity compared to previously reported non-noble metal catalysts. Nevertheless, the majority of catalysts under current investigation are in the form of powder catalysts, which exhibit a significant pressure drop across the catalyst bed due to the presence of multiple layers of powder. The current loading and unloading process is not conducive and may lead to dust blockage in the waste gas treatment system. Hence, the investigation of monolithic catalysts that possess low pressure drops, facilitate easy loading and unloading, and exhibit high mechanical strength holds practical significance in achieving an efficient pollutant gas treatment process with high throughput [39–41]. Van et al. [42] discovered that the discharge of honeycomb catalysts exhibits greater stability and ease of operation when subjected to higher voltages, making them more suitable for real-world operating conditions. In addition, the comprehensive investigation of catalyst performance under various operating conditions is still required in the application of monolithic catalysts.

Currently, a significant drawback of VOCs removal is the incomplete oxidation of the parent VOCs, resulting in the generation of by-products instead of complete oxidation to CO_2 and H_2O [43]. In some cases, this process generates toxic and harmful organic by-products and even nanoparticles [44–46]. Organic by-products, which may potentially exhibit higher toxicity levels compared to their parent VOCs, along with nanoparticles, present significant hazards to both human health and the environment. Therefore, it is imperative to characterize these by-products. Liu et al. [47] employed Mn-Fe/RGO catalysts for the purpose of mitigating nanoparticle formation. Wu et al. [48] discovered that the utilization of plasma-coupled Au/γ-Al_2O_3 nanocatalysts for the oxidation of toluene resulted in a remarkable reduction of nanoparticle emission by 99.99%. Nevertheless, limited research has been conducted to comprehensively examine the qualitative analysis of both the gaseous and particulate by-products generated from plasma catalytic systems. The complexity of decomposition pathways and the formation of intermediates in both gas and particle phases contribute significantly to the challenge of tracking and analyzing the complete degradation process in real-time. Currently, there is a lack of effective methods to address this issue.

In this study, an α-MnO_2/CHM catalyst was implemented in the DBD reactor to facilitate the decomposition of toluene. Additionally, potential pathways for toluene decomposition were suggested. The gas-phase and particle-phase products produced by the NTP combined α-MnO_2/CHM catalyst were analyzed using proton transfer reaction time-of-flight mass spectrometry (PTR-TOF-MS), particle size spectrometer (SMPS), and thermal desorption gas chromatography-mass spectrometer (TD-GC-MS). Additionally, a reaction mechanism was proposed based on the obtained results.

2. Experimental section

2.1. Preparation of materials and catalysts

In this experimental study, the amorphous α-MnO_2 catalyst was prepared in powder form using the redox precipitation method [49]. Subsequently, a specific quantity of α-MnO_2 powder catalyst and deionized water were combined and subjected to ball milling. Following this, a specific amount of aluminum sol and binder were introduced, resulting in the formation of α-MnO_2 slurry after 12 h of stirring. The cordierite honeycomb ceramic carrier, with dimensions of 150 mm × 150 mm× 30 mm, was immersed in the prepared slurry using the impregnation coating method and raised at a rate of 3 cm/min. The ceramic blocks, which had been impregnated, underwent centrifugation for a duration of 3 min at a speed of 400 revolutions per minute in a centrifugal dryer. Subsequently, they were dried in a blast oven at a temperature of 120 °C for a period of 45 min. This process was repeated twice. Finally, the catalyst underwent calcination in a muffle furnace at a temperature of 400 °C for a duration of 3 h. Subsequently, it was allowed to cool down to room temperature naturally, resulting in the formation of the monolithic catalyst. The carrier and α-MnO_2 monolithic catalyst are depicted in Fig. 1.

2.2. Characterization

A Smartlab X-ray diffractometer (Bruker D8 ADVANCE, Germany) was employed to conduct material phase identification and quantitative analysis. The samples were prepared for testing by cutting them into dimensions of 2 cm × 2 cm. The testing was conducted using a Johansson Kα1 high-resolution optical path, which included a fine-focused 9 KW rotating-target X-ray generator. The scanning range of the X-ray generator was set between 5° and 80°, with a step size of 8°/min.

The surface morphology of the samples was examined utilizing a field emission scanning electron microscope (ZEISS Gemini 300, Germany). The specimens were precisely sectioned into squares measuring 1 cm × 1 cm. Subsequently, they were affixed to the conductive tape of the sample stage and positioned within the sample chamber to facilitate testing. The distribution of the sample elements was obtained utilizing the accompanying energy spectrometer (EDS).

The chemical state of the elements present on the surface of the sample was analyzed using X-ray photoelectron spectroscopy (Thermo Fisher Scientific, USA). The samples underwent a cutting process to obtain 2 cm × 2 cm squares, which were subsequently used for testing purposes. During the experiments, the samples were exposed to Al Kα rays for irradiation. The binding energy of C1s at 284.80 eV was utilized as the energy standard for charge correction.

2.3. The NTP-MS system

The evaluation experiment comprises a VOC generation system, post-plasma-catalyzed reaction systems, and an analysis system (Fig. 2). In the system for generating VOCs, the zero air produced by the zero air generator (AADCO737, Aadco, USA) is utilized as the carrier gas. This zero air is then mixed with toluene (102 ppmv, Shanghai, Weichuang Standard Gas Co., Ltd., China) standard gas on the gas distribution platform (DSG-1000, Shanghai Haishan Intelligent Instrument Co., Ltd., China) in order to obtain the desired gas distribution for the subsequent experimental reactions. The experiment involves regulating the overall gas flow through the use of a flow meter in the gas distribution platform. Additionally, the concentration of toluene is controlled by adjusting the flow rates of both the toluene and carrier gas. In the context of this experiment, the adjustable range for total gas flow is 100–2000 mL/min and the gas hourly space velocity (GHSV) is 3822–19108 h^{-1}.

The reaction gas, which has been prepared in advance, is introduced into the plasma catalytic reaction system that has been designed by the

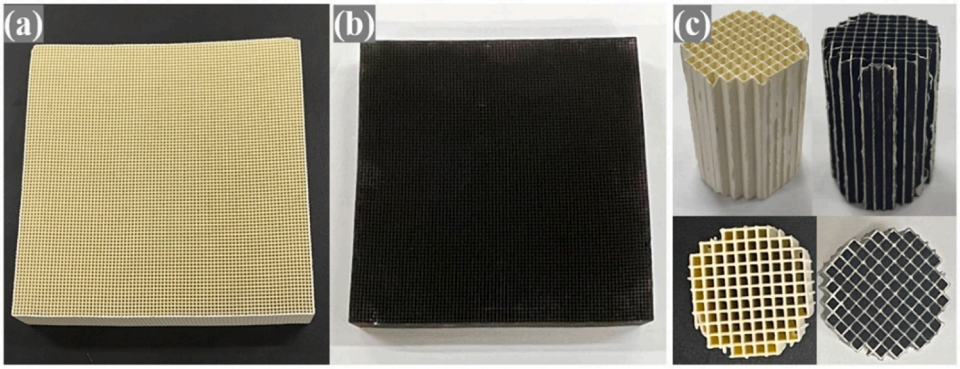

Fig. 1. (a) Blank carrier; (b) α-MnO_2 monolithic catalyst; (c) Blank carrier and α-MnO_2 monolithic catalyst after cutting for activity testing.

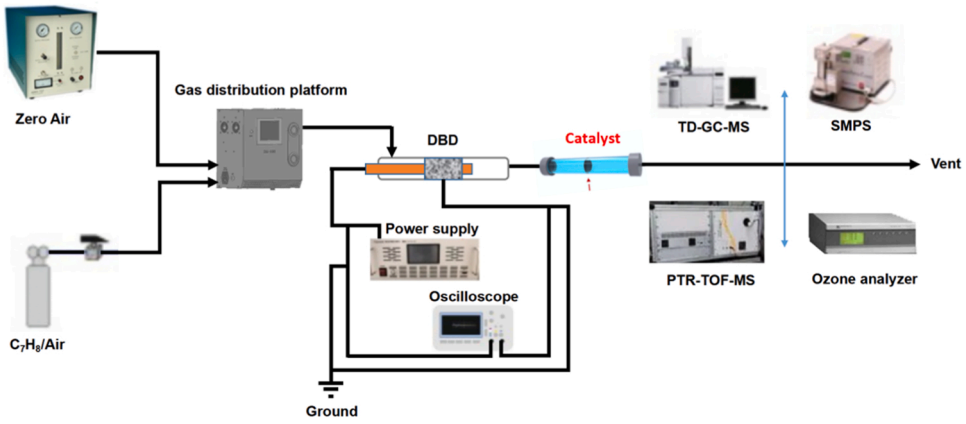

Fig. 2. Schematic diagram of the experimental setup.

researchers. The dielectric barrier discharge (DBD) reactor is comprised of a quartz tube with an outer diameter of 6 mm and an inner diameter of 4 mm. It includes a grounding electrode, which is an 8 mm long aluminum foil wrapped around the quartz tube, and a high-pressure electrode, which is a 2 mm diameter stainless steel rod positioned on the shaft of the quartz tube. Connect the high-voltage electrode to the high-voltage AC plasma generator (CTP-2000, Suman Plasma Technology, China). The plasma generator maintains an output frequency of 10 kHz throughout the duration of the experiment. A digital oscilloscope (DSO6032A, Agilent Technologies, USA) is employed to capture and analyze the voltage and current signals associated with the discharge process. The catalyst, with dimensions of Φ20 × 20 mm, is introduced into the catalytic reactor and positioned downstream of the DBD reactor. The external catalytic reactor is equipped with a gas flow bypass in parallel, allowing for direct testing of the performance of individual plasma degradation of toluene by switching the gas valve.

In the gas composition analysis system, the concentration of toluene and the intermediate products of the reaction are monitored using a proton transfer reaction time-of-flight mass spectrometry (PTR-TOF-MS) instrument that was independently developed by the laboratory. The concentration of O_3 is measured by the ozone analyzer (EC9810, Ecotech, Australia), CO_2 and CO are determined by the CO_X analyzer (Smart Pro10, Shandun Technology (Shenzhen) Co., Ltd., China). Additionally, the number and composition of by-product particles are measured using a scanning mobility particle size spectrometer (SMPS, DMA3081/CPC3776, GRIMM, Germany) and a thermal desorption system (TD3.5$^+$, Gerstel, Maestro1, Germany) in combination with a gas chromatography-mass spectrometry (8890–5977B GC/MS, Agilent, USA) instrument. Please see part 1 in the supporting materials for detailed instructions.

2.4. Calculations

As shown in Fig. 3, the average discharge power (P) delivered to the reactor was obtained by integrating the product of the voltage (V) and current (I) over one cycle, as in Eq. (1).

$$\text{Discharge Power} P(W) = \frac{1}{T}\int_0^T V(t) \times I(t) \times dt \tag{1}$$

In this way, the specific input energy (SIE) was calculated, as in Eq. (2):

$$\text{Specific Input Energy}, SIE(J/L) = \frac{P(W)}{Q(\frac{L}{\min})} \times 60\left(\frac{S}{\min}\right) \tag{2}$$

The EA conversion (η (%)) and CO_X selectivity were calculated using Eqs. (3) and (4), respectively.

$$EA \quad Conversion\eta(\%) = \frac{C^{in}_{C_7H_8} - C^{out}_{C_7H_8}}{C^{in}_{C_7H_8}} \times 100\% \tag{3}$$

$$CO_X \quad \text{Selectivity}, S_{CO_X}(\%) = \frac{C_{CO} + C_{CO_2}}{7\left(C^{in}_{C_7H_8} - C^{out}_{C_7H_8}\right)} \times 100\% \tag{4}$$

where C_{CO_X} is the concentration of CO_X after the reaction, $C^{in}_{C_7H_8}$ and $C^{out}_{C_7H_8}$ are the concentrations of EA in the inlet and outlet of the reactor.

The ozone removal efficiency (%) was calculated using Eq. (5) below.

$$\text{Ozone removal efficiency} \quad X_{O_3}(\%) = \frac{C_{in} - C_{out}}{C_{in}} \times 100\% \tag{5}$$

Here, C_{in} and C_{out} (ppm) as the ozone concentration before and after

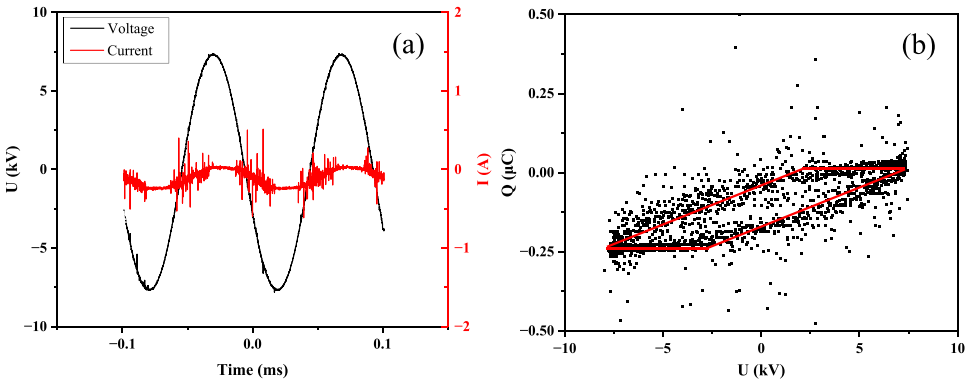

Fig. 3. (a) The discharge current and voltage waveforms of toluene in the air; (b) Lissajous figure of DBD.

reaction.

2.5. Statistical analysis

Experimental data were collected, analyzed and plotted using Origin 2022, and all data are expressed as mean ± standard deviation of at least three replicates.

3. Results and discussion

3.1. Catalyst characterization

3.1.1. XRD analysis

Fig. 4 presents the XRD patterns of the α-MnO_2 monolithic catalyst and the blank carrier that were prepared. It is evident that the characteristic peaks of the cordierite blank carrier and α-MnO_2 monolithic catalyst exhibit minimal variation in their positions. The cordierite peaks predominantly consist of a combination of its constituent components, namely alumina, silicon oxide, and magnesium oxide, resulting in multiple peaks [50]. However, there is a notable alteration in the peak intensity and a substantial decrease in the crystallinity of the α-MnO_2 monolithic catalyst. This can be attributed to the amorphous nature and low crystallinity of α-MnO_2, as well as the significant reduction in crystallinity caused by its loading onto the monolithic catalyst.

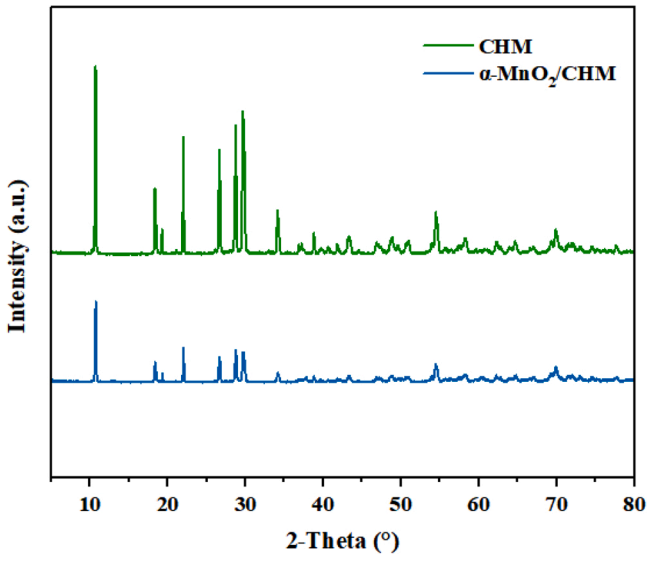

Fig. 4. XRD patterns of blank carrier and α-MnO_2 monolithic catalyst.

3.1.2. SEM and EDS

SEM analysis was conducted to examine the microstructure and surface morphology of the catalysts. Fig. 5 displays the SEM images of both the blank carrier and the α-MnO_2 monolithic catalyst. Fig. 5a illustrates that the cordierite blank carrier, characterized by its rough surface, is devoid of any extraneous substances. When the catalyst was introduced, as depicted in Figs. 5b and 5c, the α-MnO_2 particles effectively enveloped the initial monolithic surface and exhibited a homogeneous dispersion on the carrier. This assertion is further supported by the elemental mapping images obtained through EDS of selected regions of the α-MnO_2 monolithic catalyst, as shown in Fig. 6. The presence of Mn, Al, and Mg on the catalyst surface can be observed, indicating the existence of Mn oxide, Al oxide, and Mg oxide, respectively. All of the measurement results indicate the successful deposition of the amorphous α-MnO_2 active loaded onto the surface of the cordierite blank carrier.

3.1.3. XPS

The oxidation states of the elements on the catalyst surface were also determined through XPS. Fig. 7a displays the comprehensive scanned full spectrum of the surface elements present in the α-MnO_2 monolithic catalyst. The spectrum reveals the presence of Mn at an energy range of 630–660 eV, along with the relative percentages of C, O, Al, Mn, and Mg elements, which are 24.70%, 41.47%, 18.02%, 6.52%, and 9.29%, respectively. These percentages indicate the coverage of the active component, Mn oxide. Fig. 7b displays the XPS spectrum of Mn 2p in the catalyst, wherein the Mn 2p3/2 peak exhibits a splitting into two distinct peaks at 642.6 eV and 644.9 eV. These peaks are attributed to the presence of Mn^{3+} and Mn^{4+} species, respectively. Among the various elements, the presence of Mn^{3+} is significantly higher, accounting for 82.25% more. The catalytic process involving the interconversion of Mn^{4+}/Mn^{3+} can generate a greater number of active sites and active species. Typically, a significant presence of low-valent Mn indicates a substantial amount of oxygen vacancies on the surface. This condition facilitates the transportation of oxygen, thereby promoting the production of active oxygen and contributing to the extensive oxidative degradation of toluene and its intermediates.

3.2. The impact of reaction conditions on the efficiency of toluene removal

The impact of the flow of reaction gas on the reaction of plasma and plasma-catalyzed systems is illustrated in Fig. 8. It is evident that the enhancement of reaction gas flow does not promote the degradation of toluene through plasma. This is due to the decrease in residence time of toluene in the discharge area or on the catalyst surface caused by the increased gas flow. Consequently, the likelihood of collision between toluene molecules and the active material is reduced. Plasma and plasma catalytic reactions are known to be influenced by the quantity of

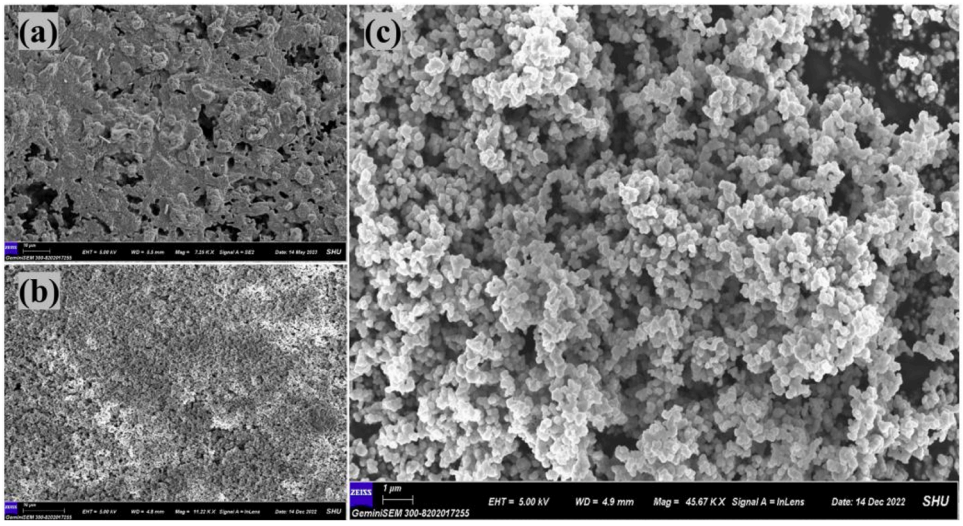

Fig. 5. SEM images of (a) the blank support and (b,c) α-MnO_2 monolithic catalyst.

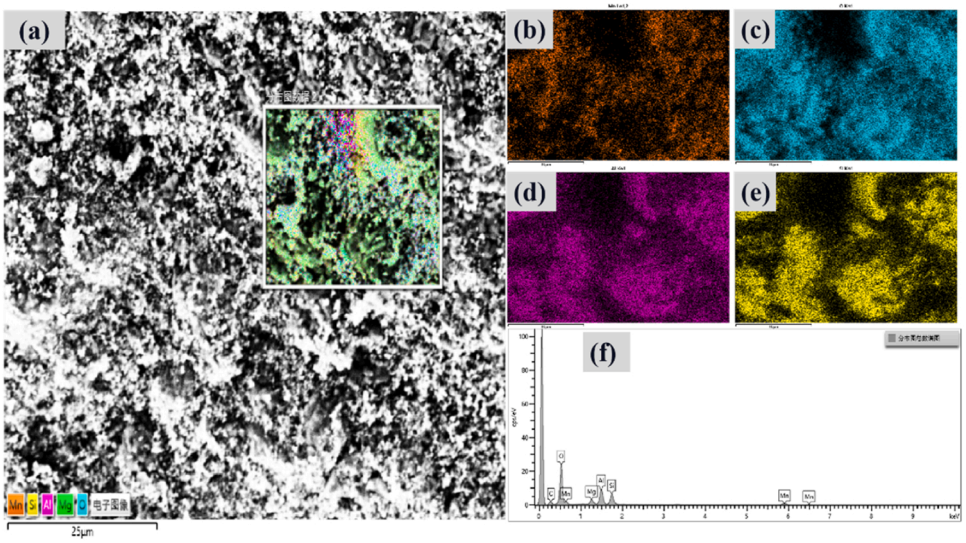

Fig. 6. EDS element mapping image depicting a selected region of the α-MnO_2/CHM catalyst. (a) EDS layered image;(b) Mn;(c) O;(d) Al;(e) Si;(f) Spectrogram of the total number of distribution maps.

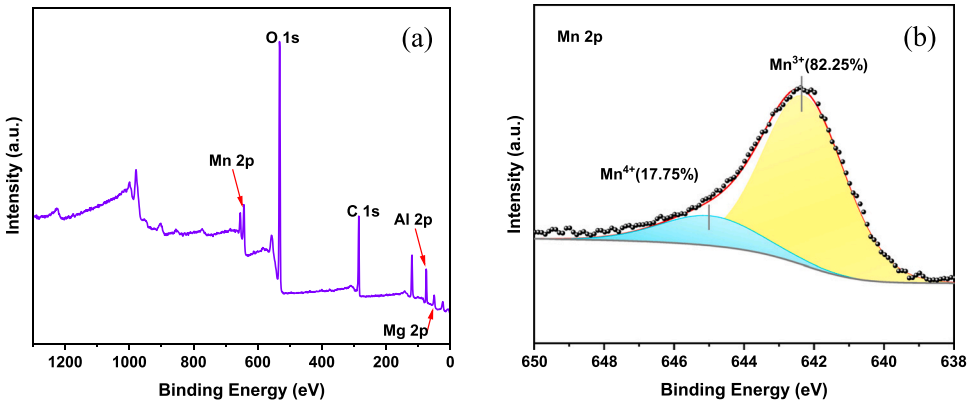

Fig. 7. Total scanning spectrum of elements (a) and Mn 2p XPS spectrum (b) of α-MnO_2 monolithic catalyst.

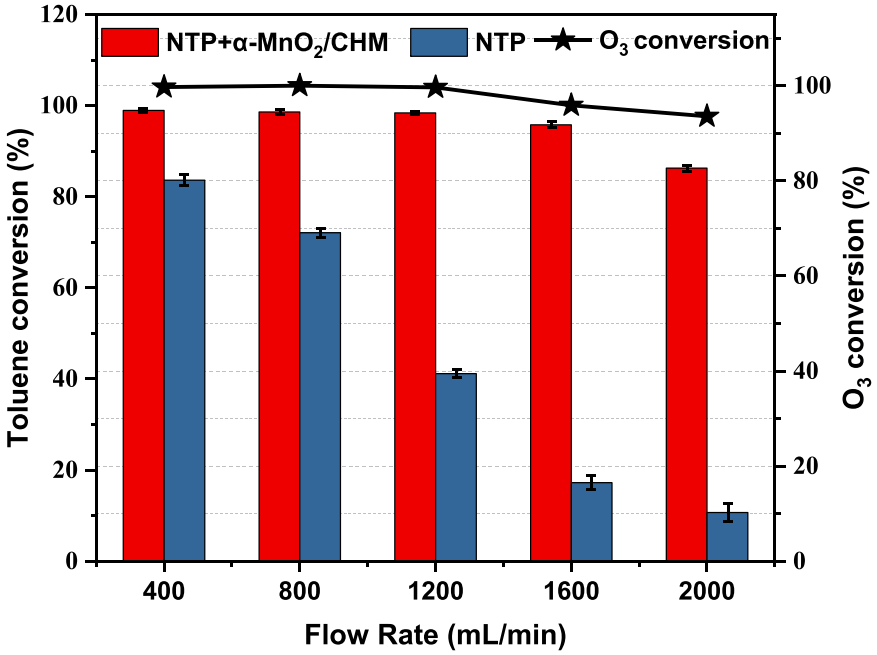

Fig. 8. Effect of the impact of reaction flow rate on both plasma and plasma-catalyzed systems (Toluene concentration:100 ppm; temperature: 26 °C; input voltage:52 kV).

reaction gas flow [51]. However, in plasma catalytic systems, the presence of catalysts mitigates the impact of changes in flow. The aforementioned observation demonstrates that the plasma catalytic system exhibits a commendable capability in processing high-throughput toluene gas. This capability serves as a compensatory mechanism to counteract the negative impacts caused by an elevated flow rate of plasma. The α-MnO_2 monolithic catalyst exhibits remarkable efficacy in eliminating ozone. It effectively removes the by-product O_3 produced by plasma, resulting in a final ozone removal rate exceeding 90%.

The impact of the initial toluene concentration on the plasma-catalyzed reaction is depicted in Fig. 9. It is evident that, under constant discharge power and reaction gas flow conditions, the initial concentration of VOCs has an impact on their degradation effectiveness. Whether using plasma alone or plasma-catalyzed methods, it has been observed that increasing the initial concentration of toluene leads to a reduction in the removal rate. The reason may be due to that the applied voltage of the plasma during the discharge process directly affects the amount and intensity of physicochemical effects, such as active substances, energetic electrons, and UV rays in the plasma [52], and the production of energetic electrons and active substances is limited under the same power conditions. As the initial concentration of toluene increases, the likelihood of each toluene molecule colliding with the active substance decreases [53], resulting in a decrease in the degradation rate. After incorporating catalyst synergy, the impact of concentration

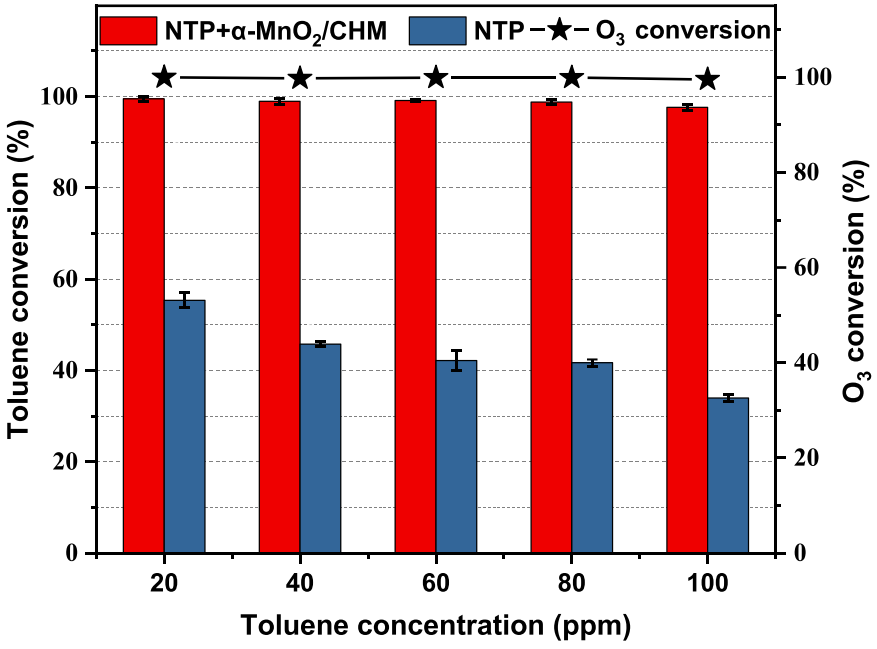

Fig. 9. Effect of initial toluene concentration on plasma and plasma-catalyzed system (Reaction gas flow rate: 1200 mL/min; temperature: 26 °C; input voltage:52 kV).

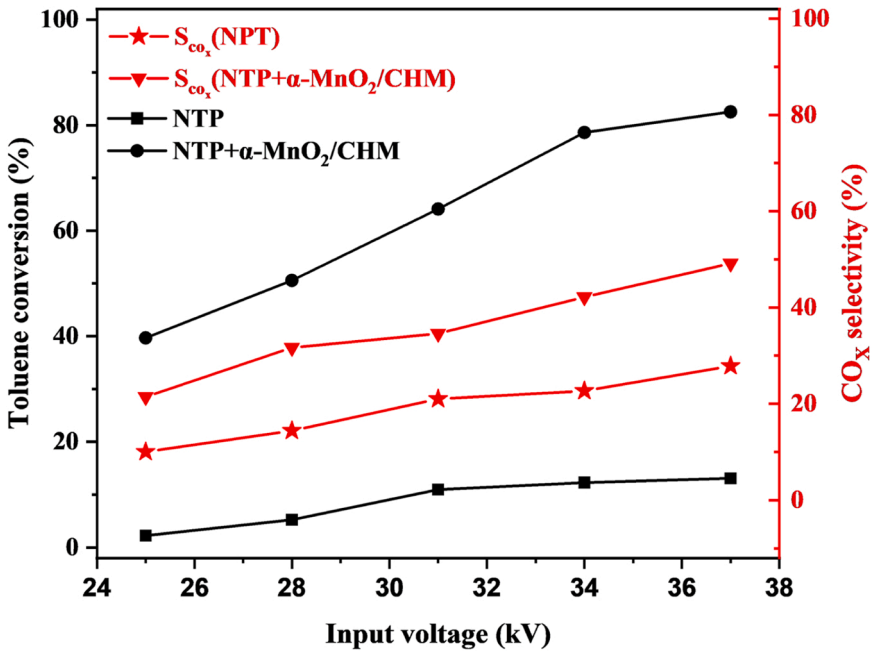

Fig. 10. Effect of discharge power on plasma and plasma-catalyzed systems (Reaction gas flow rate: 1200 mL/min; temperature: 26 °C; toluene concentration: 50 ppm).

variation on the degradation rate is considerably mitigated, thereby facilitating the enhancement of energy efficiency.

Fig. 10 illustrates the relationship between the efficiency toluene degradation and the input voltage and carbon balance in both single plasma and plasma-catalyzed systems. The degradation rate of toluene exhibits a positive correlation with the discharge power. This phenomenon can be attributed to the amplification of plasma discharge power, resulting in the generation of a larger quantity of high-energy electrons and active compounds within the plasma region. Consequently, this promotes the decomposition of toluene [54]. In plasma catalytic systems, the degradation rate of toluene and the selectivity towards carbon are enhanced. This result demonstrates that the presence of a catalyst greatly enhances the degradation rate and energy efficiency of toluene, thereby promoting its deep oxidation.

Under optimal conditions, the catalyst alone has no catalytic ability when compared with a plasma catalytic system (as shown in Fig. S1).

3.3. *Exploring the products generated by plasma catalysis*

Ozone is one of the key gas phase byproducts of plasma reactions, and it mainly comes from the dissociation of oxygen molecules in the air [55]. Fig. S2 shows the ozone removal efficiency in the exhaust gas of plasma catalytic system changes with energy density, and clearly, ozone has a high removal efficiency under a wide energy density range. In general, the ozone produced by plasma increases with the increase of energy density [56]. After catalyst introduction, the ozone content in the exhaust gas of the entire plasma catalytic system decreases significantly, and the removal efficiency is more than 99%, indicating ozone is efficiently removed through catalyst used.

The generation of aerosols has been observed when VOCs are treated with plasma [57–59]. In this study, a SMPS was employed to observe and analyze the particle size distribution ranging from 10 to 1000 nm, which was generated through the degradation of toluene under both plasma and plasma catalytic systems. Fig. 11 illustrates the relationship between particulate matter number concentration and experimental conditions. It can be seen that more particles were generated during the process of plasma degradation of toluene with compared without catalyst. The number concentration of particles increases as the discharge power increases. It means that the increased discharge power promoting the particle formation. Furthermore, it can be observed that a decrease in toluene concentration leads to a corresponding decrease in the number of particles, suggesting a correlation between particle formation

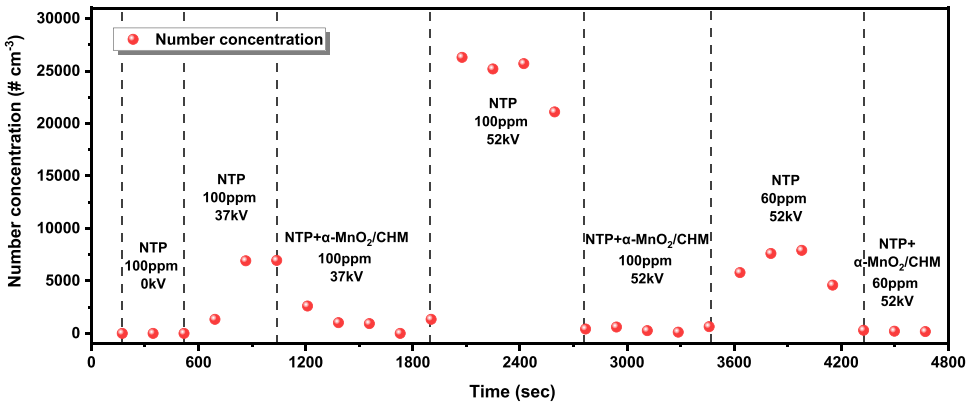

Fig. 11. Variation of the particulate matter number concentration in relation to experimental conditions.

and the toluene inlet. However, after switching to plasma catalysis, the emission of nanoparticles was reduced by 99%, suggesting an excellent particulate removal effect for the catalyst.

The products of were detected and analyzed degradation a plasma-only system and plasma synergistic monolithic catalyst system. The analysis system conducted online using by PTR-TOF-MS, and resulting obtained are presented shown in Fig. 12. It can be seen that when plasma alone is used to degrade toluene, the tail gas contains a large number of intermediate products, such as formaldehyde (HCHO), methanol (CH_3OH), acetone (C_3H_6O), acetaldehyde (CH_3CHO), ketene (C_2H_2O), formic acid (HCOOH), acetic acid (CH_3COOH), benzene (C_6H_6), benzaldehyde (C_7H_6O), etc. After the introduction of the catalyst, the formation of by-products was effectively inhibited, and the content of by-products in the tail gas was significantly reduced. Among them, methanol, acetone, acetic acid and benzaldehyde are almost completely degraded. This phenomenon can be attributed to the significant generation of active oxygen species at the oxygen vacancy on the catalyst's surface during ozone decomposition. Consequently, the reaction rate of the oxidation reaction is enhanced, and the by-products undergo further deep oxidation by the active oxygen species. Ultimately, this process leads to the production of CO_2, CO, and H_2O.

In order to investigate the aerosols produced during the plasma treatment of toluene, the particulate matter present in the exhaust gas was collected using a quartz membrane. The collected samples were then analyzed for their particulate matter composition using TD-GC-MS. Fig. 13 displays the total ion chromatogram of the particle phase obtained from both the plasma and plasma-catalyzed systems. In the plasma catalytic system, the catalyst effectively inhibits the formation of aerosols, and the particulate matter in the exhaust gas is significantly reduced. This finding implies that the particulate matter generated through plasma treatment of toluene has the potential to accumulate or adhere to the catalyst surface, and subsequently undergo further degradation through the synergistic effects of plasma catalysis.

3.4. Analysis of the production mechanism

The mechanism of plasma catalytic degradation of toluene was inferred by combining the product analysis results of gas and particle phases. In general, the degradation of toluene in post-mounted plasma catalytic systems is accomplished through a two-part reaction [44]. Firstly, when an electric field is applied to the plasma, a significant number of high-energy electrons are generated during the gas discharge. These high-energy electrons then interact with molecules such as N_2 and O_2 in the carrier gas, resulting in the production of various active substances including hydroxyl radicals, excited nitrogen, and reactive oxygen species [60]. These active substances subsequently undergo collisions with toluene and its intermediate products, leading to chemical reactions. Finally, the aforementioned intermediates undergo oxidation and degradation processes facilitated by highly reactive free radicals and oxidizing agents, resulting in the formation of smaller molecules such as CO_2, CO and H_2O by highly active free groups and oxidizing substances. The degradation path diagram of this degradation process is shown in Fig. 14a. C-H in methyl groups is easily broken by high-energy electrons to form benzyl radicals, which can react with various oxygen to form benzaldehyde, benzyl formate and benzyl alcohol. C-C bonds undergo degradation upon exposure to high-energy electrons, resulting in the formation of methyl and phenyl radicals [61]. Excitation of methyl groups can lead to polymerization or the facile formation of acetone and formic acid in the presence of reactive oxygen species. Phenyl radicals and methyl radicals have the potential to undergo further reactions, resulting in the formation of o-xylene, p-xylene [62,63] as well as various oxygen radicals that can lead to the production of p-xylene and m-dimethyl phenol. In addition, the formation of toluene can occur through the reaction with NO_2 radicals. All aromatic intermediates are susceptible to the attack of high-energy electrons or reactive substances, resulting in subsequent oxidation of the ring and the formation of CO_2 and H_2O. The subsequent stage involves the execution of the reaction on the catalyst's surface, as shown in Fig. 14b. In plasma catalytic systems, the adsorption of toluene and its intermediates onto the catalyst surface occurs prior to the oxidation process following plasma treatment [64]. The oxidation of toluene and its intermediates occurs through the interaction with active oxygen species present on the catalyst's surface. These active oxygen species are primarily derived from ozone, and the ozone generated in the discharge zone can be decomposed by the catalyst, resulting in the formation of excited oxygen atoms. The enhancement of toluene degradation in

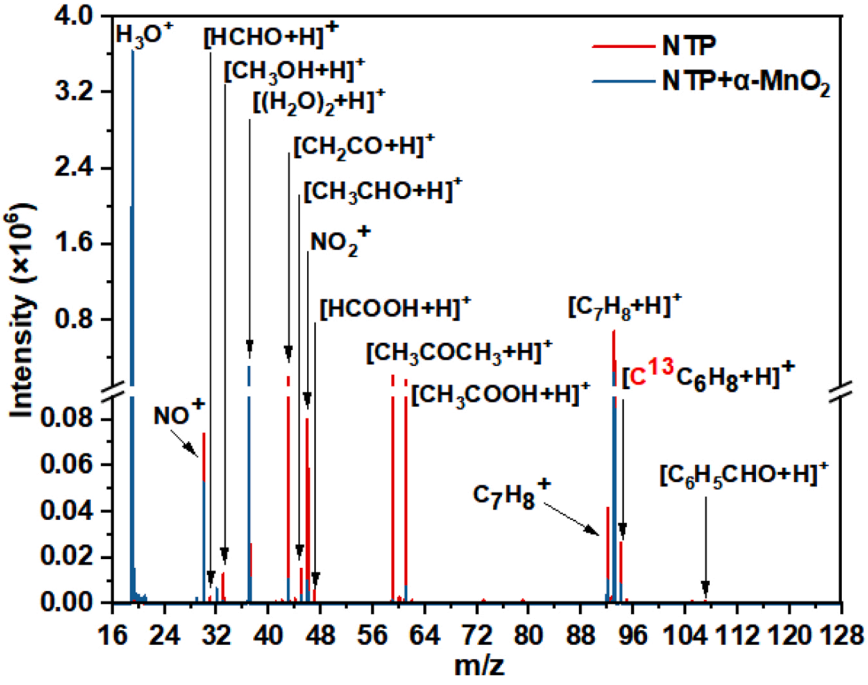

Fig. 12. PTR-TOF-MS spectra of gas-phase by-products generated by plasma and plasma-catalyzed systems.

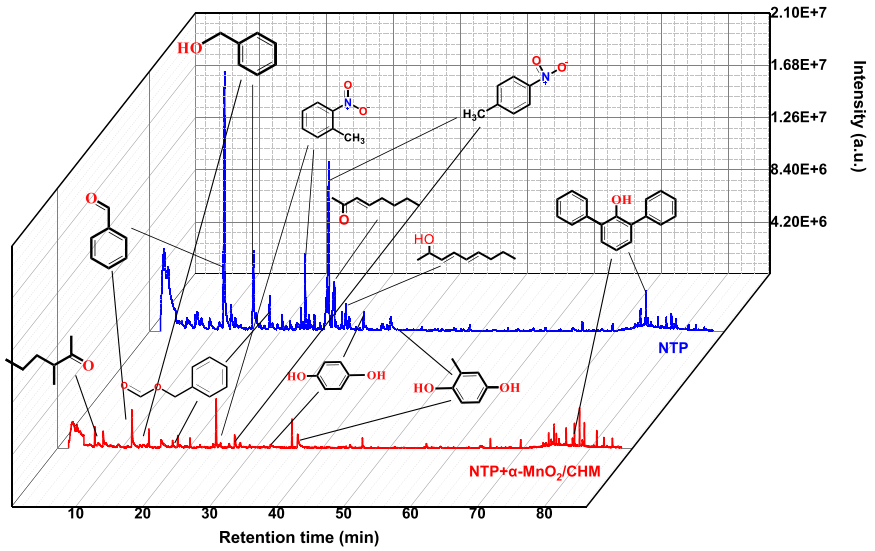

Fig. 13. Total ion flow chromatography of particle phase products generated by plasma and plasma catalytic system.

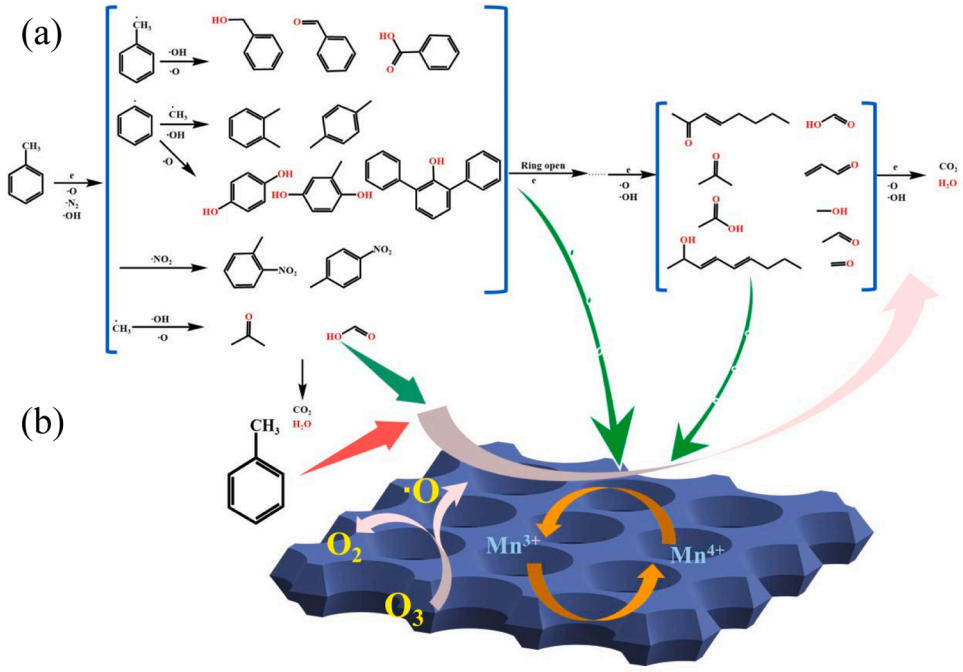

Fig. 14. The Degradation pathway of toluene in a Plasma Catalytic System: (a) reaction in plasma and (b) reaction on catalyst surface.

plasma catalytic systems is intricately linked to the catalytic process of O_3 [65]. O_3 has been documented to have a significant impact on the degradation process of toluene. The in-situ decomposition of O_3 results in the generation of atomic oxygen, which has the capability to engage in reactions with various contaminants [66]. Furthermore, the catalyst undergoes a mutual conversion of Mn^{4+}/Mn^{3+}, resulting in the generation of additional active sites. The transfer of oxygen from these active species [67] occurs through this cycle, and the presence of oxygen vacancies facilitates the formation of reactive oxygen species. The XPS characterization of the catalyst in this study indicated that the α-MnO_2 monolithic catalyst exhibits a significant Mn^{3+} content and a substantial presence of oxygen vacancies. Consequently, it exhibits high mobility of reactive oxygen, which contributes to the extensive oxidative degradation of toluene and its intermediates.

4. Conclusions

The dielectric barrier discharge reactor, combined with an α-MnO_2 integral catalyst, was used to construct a plasma catalytic system. This system was applied to the degradation of toluene. The experimental results show that the plasma catalytic system effectively degrades toluene. Compared to a single plasma, the toluene degradation rate, carbon selectivity, and energy efficiency are significantly improved in the plasma catalytic system due to the synergistic effect of the monolithic catalyst. When the concentration is 100 ppm, the flow rate is 1.2 L/min, and the power is 6.36 W, the toluene degradation efficiency reaches 98%. Among them, increasing the initial concentration of VOCs is not conducive to the degradation of organic matter through plasma-catalyzed reactions. However, introducing a catalyst within a certain concentration range can mitigate the impact of concentration changes.

Gas flow is another important factor that influences plasma-catalyzed reactions. Selecting moderate flow conditions is beneficial for achieving a high removal rate of VOCs while minimizing the formation of by-products. The increase in discharge voltage can significantly enhance the final outcome of the plasma-catalyzed reaction. In addition, the presence of a catalyst significantly inhibits by-product emissions and greatly reduces the generation of ozone and particulate matter. The components of gas phase and granular phase products were analyzed, and a plausible degradation pathway for toluene in the PPC process was proposed. The destruction of toluene can be summarized in two ways: the direct degradation of energetic electrons and reactive radicals in the discharge region, and the deep oxidation of active oxygen species on the catalyst surface. This study establishes a foundation for the treatment of VOCs in industrial applications using α-MnO_2 monolithic catalysts.

CRediT authorship contribution statement

Qianqian Yan: Investigation, Writing- Original draft preparation. **Jiafan Ji:** Resources, Data curation. **Yi Chen:** Data curation, Formal analysis. **Gaosheng Zhao:** Visualization, Software. **Bing Jia:** Methodology. **Li Xu:** Supervision, Validation. **Ping Cheng:** Conceptualization Writing - Reviewing and Editing, Funding acquisition.

Declaration of Competing Interest

The authors declare that they have no known competing financial interests or personal relationships that could have appeared to influence the work reported in this paper.

Data Availability

Data will be made available on request.

Acknowledgments

The authors gratefully acknowledge financial support from the National Natural Science Foundation of China (No. 42277217, 41877374) and Shanghai Science and Technology development Foundation (No.21SQBS01900).

Appendix A. Supporting Information

Supplementary data associated with this article can be found in the online version at doi:10.1016/j.apcatb.2023.123530.

References

[1] L. Hui, X. Liu, Q. Tan, M. Feng, J. An, Y. Qu, Y. Zhang, N. Cheng, VOC characteristics, sources and contributions to SOA formation during haze events in Wuhan, Central China, Sci. Total Environ. 650 (2019) 2624–2639.
[2] W. Wei, Y. Li, Y. Wang, S. Cheng, L. Wang, Characteristics of VOCs during haze and non-haze days in Beijing, China: Concentration, chemical degradation and regional transport impact, Atmos. Environ. 194 (2018) 134–145.
[3] R.-J. Huang, Y. Zhang, C. Bozzetti, K.-F. Ho, J.-J. Cao, Y. Han, K.R. Daellenbach, J. G. Slowik, S.M. Platt, F. Canonaco, High secondary aerosol contribution to particulate pollution during haze events in China, Nature 514 (2014) 218–222.
[4] P. Wu, X. Jin, Y. Qiu, D. Ye, Recent progress of thermocatalytic and photo/thermocatalytic oxidation for VOCs purification over manganese-based oxide catalysts, Environ. Sci. Technol. 55 (2021) 4268–4286.
[5] X. Zhang, B. Gao, A.E. Creamer, C. Cao, Y. Li, Adsorption of VOCs onto engineered carbon materials: A review, J. Hazard. Mater. 338 (2017) 102–123.
[6] H. Wang, B. Wang, J. Li, T. Zhu, Adsorption equilibrium and thermodynamics of acetaldehyde/acetone on activated carbon, Sep. Purif. Technol. 209 (2019) 535–541.
[7] B. Belaissaoui, Y. Le Moullec, E. Favre, Energy efficiency of a hybrid membrane/condensation process for VOC (Volatile Organic Compounds) recovery from air: A generic approach, Energy 95 (2016) 291–302.
[8] W. Yang, H. Zhou, C. Zong, Y. Li, W. Jin, Study on membrane performance in vapor permeation of VOC/N2 mixtures via modified constant volume/variable pressure method, Sep. Purif. Technol. 200 (2018) 273–283.
[9] Z. Zhang, Z. Jiang, W. Shangguan, Low-temperature catalysis for VOCs removal in technology and application: A state-of-the-art review, Catal. Today 264 (2016) 270–278.
[10] C. Yang, G. Miao, Y. Pi, Q. Xia, J. Wu, Z. Li, J. Xiao, Abatement of various types of VOCs by adsorption/catalytic oxidation: A review, Chem. Eng. J. 370 (2019) 1128–1153.
[11] J. Guo, C. Lin, C. Jiang, P. Zhang, Review on noble metal-based catalysts for formaldehyde oxidation at room temperature, Appl. Surf. Sci. 475 (2019) 237–255.
[12] W. Zou, B. Gao, Y.S. Ok, L. Dong, Integrated adsorption and photocatalytic degradation of volatile organic compounds (VOCs) using carbon-based nanocomposites: A critical review, Chemosphere 218 (2019) 845–859.
[13] Z. Shayegan, C.-S. Lee, F. Haghighat, TiO2 photocatalyst for removal of volatile organic compounds in gas phase–A review, Chem. Eng. J. 334 (2018) 2408–2439.
[14] A.H. Mamaghani, F. Haghighat, C.-S. Lee, Photocatalytic oxidation technology for indoor environment air purification: The state-of-the-art, Appl. Catal. B: Environ. 203 (2017) 247–269.
[15] J.M. Estrada, O.I. Bernal, M.C. Flickinger, R. Muñoz, M.A. Deshusses, Biocatalytic coatings for air pollution control: A proof of concept study on VOC biodegradation, Biotechnol. Bioeng. 112 (2015) 263–271.
[16] J.C. Whitehead, Plasma catalysis: A solution for environmental problems, Pure Appl. Chem. 82 (2010) 1329–1336.
[17] S.K.P. Veerapandian, N. De Geyter, J.-M. Giraudon, J.-F. Lamonier, R. Morent, The use of zeolites for VOCs abatement by combining non-thermal plasma, adsorption, and/or catalysis: a review, Catalysts 9 (2019) 98.
[18] J. Li, S. Yao, Z. Wu, NOx production in plasma reactors by pulsed spark discharges, J. Phys. D: Appl. Phys. 53 (2020), 385201.
[19] K. Shang, X. Wang, J. Li, H. Wang, N. Lu, N. Jiang, Y. Wu, Synergetic degradation of Acid Orange 7 (AO7) dye by DBD plasma and persulfate, Chem. Eng. J. 311 (2017) 378–384.
[20] K. Shang, M. Wang, B. Peng, J. Li, N. Lu, N. Jiang, Y. Wu, Characterization of a novel volume-surface DBD reactor: discharge characteristics, ozone production and benzene degradation, J. Phys. D: Appl. Phys. 53 (2019), 065201.
[21] S. Hoseini, N. Rahemi, S. Allahyari, M. Tasbihi, Application of plasma technology in the removal of volatile organic compounds (BTX) using manganese oxide nano-catalysts synthesized from spent batteries, J. Clean. Prod. 232 (2019) 1134–1147.
[22] N. Jiang, C. Qiu, L. Guo, K. Shang, N. Lu, J. Li, Y. Zhang, Y. Wu, Plasma-catalytic destruction of xylene over Ag-Mn mixed oxides in a pulsed sliding discharge reactor, J. Hazard. Mater. 369 (2019) 611–620.
[23] B. Lee, D.-W. Kim, D.-W. Park, Dielectric barrier discharge reactor with the segmented electrodes for decomposition of toluene adsorbed on bare-zeolite, Chem. Eng. J. 357 (2019) 188–197.
[24] A. Vandenbroucke, R. Morent, N. De Geyter, C. Leys, Decomposition of Trichloroethylene with Plasma-catalysis: A review, J. Adv. Oxid. Technol. 14 (2011) 165–173.
[25] O. Karatum, M.A. Deshusses, A comparative study of dilute VOCs treatment in a non-thermal plasma reactor, Chem. Eng. J. 294 (2016) 308–315.
[26] K.L. Pan, G.T. Pan, S. Chong, M.B. Chang, Removal of phenol from gas streams via combined plasma catalysis, J. Ind. Eng. Chem. 52 (2017) 108–120.
[27] S. Dong, Y. Wang, J. Yang, J. Cao, L. Su, X. Wu, L.-c. Nengzi, S. Liu, Performance and mechanism analysis of degradation of toluene by DBD plasma-catalytic method with MnOx/Al2O3 catalyst, Fuel 319 (2022), 123721.
[28] T. Chang, C. Ma, Z. Shen, S.K. Veerapandian, Y. Huang, N. De Geyter, R. Morent, Mn-based catalysts for post non-thermal plasma catalytic abatement of VOCs: a review on experiments, simulations and modeling, Plasma Chem. Plasma Process. 41 (2021) 1239–1278.
[29] E. Rezaei, J. Soltan, Low temperature oxidation of toluene by ozone over MnOx/γ-alumina and MnOx/MCM-41 catalysts, Chem. Eng. J. 198 (2012) 482–490.
[30] E. Rezaei, J. Soltan, N. Chen, Catal. Oxid. toluene Ozone alumina Support. Manganese oxides: Eff. Catal. Load., Appl. Catal. B: Environ. 136 (2013) 239–247.
[31] R. Liu, S. Liu, H. Ding, D. Zhao, J. Fu, Y. Zhang, W. Huo, G.K. Li, Unveiling the role of atomically dispersed active sites over amorphous iron oxide supported Pt catalysts for complete catalytic ozonation of toluene at low temperature, Ind. Eng. Chem. Res. 60 (2021) 3881–3892.
[32] C. He, Y. Wang, Z. Li, Y. Huang, Y. Liao, D. Xia, S. Lee, Facet engineered α-MnO2 for efficient catalytic ozonation of odor CH3SH: oxygen vacancy-induced active centers and catalytic mechanism, Environ. Sci. Technol. 54 (2020) 12771–12783.
[33] X. Li, J. Ma, L. Yang, G. He, C. Zhang, R. Zhang, H. He, Oxygen vacancies induced by transition metal doping in γ-MnO2 for highly efficient ozone decomposition, Environ. Sci. Technol. 52 (2018) 12685–12696.
[34] D.A. Aguilera, A. Perez, R. Molina, S. Moreno, Cu–Mn and Co–Mn catalysts synthesized from hydrotalcites and their use in the oxidation of VOCs, Appl. Catal. B: Environ. 104 (2011) 144–150.
[35] B. Dhandapani, S.T. Oyama, Gas phase ozone decomposition catalysts, Appl. Catal. B: Environ. 11 (1997) 129–166.
[36] Z. Ye, J.-M. Giraudon, N. De Geyter, R. Morent, J.-F. Lamonier, The design of MnO x based catalyst in post-plasma catalysis configuration for toluene abatement, Catalysts 8 (2018) 91.
[37] Y. Wang, D. Yang, S. Li, L. Zhang, G. Zheng, L. Guo, Layered copper manganese oxide for the efficient catalytic CO and VOCs oxidation, Chem. Eng. J. 357 (2019) 258–268.
[38] W. Hong, Y. Liu, T. Zhu, H. Wang, Y. Sun, F. Shen, X. Li, Promoting the Catalytic Ozonation of Toluene by Introducing SO42–into the α-MnO2/ZSM-5 Catalyst to Tune Both Oxygen Vacancies and Acid Sites, Environ. Sci. Technol. 56 (2022) 15695–15704.
[39] F.J. Maldonado-Hódar, S. Morales-Torres, F. Ribeiro, E.R. Silva, A.F. Pérez-Cadenas, F. Carrasco-Marín, F.A.C. Oliveira, Development of carbon coatings for

cordierite foams:: An alternative to cordierite honeycombs, Langmuir 24 (2008) 3267–3273.
[40] V. Tomasic, F. Jovic, State-of-the-art in the monolithic catalysts/reactors, Appl. Catal. a-Gen. 311 (2006) 112–121.
[41] C. Chen, W. Zhang, J. Qiu, A. Jia, M. Luo, Catalytic Decomposition of Ozone by Manganese Oxide Supported on Cordierite Honeycomb Ceramics, Chin. J. Appl. Chem. 37 (2020) 1293–1300.
[42] V.T. Nguyen, D.B. Nguyen, Y.S. Mok, M.M. Hossain, S. Saud, K.H. Yoon, D.K. Dinh, S. Ryu, H. Jeon, S.B. Kim, Removal of ethyl acetate in air by using different types of corona discharges generated in a honeycomb monolith structure coated with Pd/γ-alumina, J. Hazard. Mater. 416 (2021), 126162.
[43] X.B. Zhu, X. Gao, R. Qin, Y.X. Zeng, R.Y. Qu, C.H. Zheng, X. Tu, Plasma-catalytic removal of formaldehyde over Cu-Ce catalysts in a dielectric barrier discharge reactor, Appl. Catal. B-Environ. 170 (2015) 293–300.
[44] X. Zhu, S. Liu, Y. Cai, X. Gao, J. Zhou, C. Zheng, X. Tu, Post-plasma catalytic removal of methanol over Mn–Ce catalysts in an atmospheric dielectric barrier discharge, Appl. Catal. B: Environ. 183 (2016) 124–132.
[45] M.N. Dinh, J.-M. Giraudon, A.M. Vandenbroucke, R. Morent, N. De Geyter, J.-F. Lamonier, Post plasma-catalysis for total oxidation of trichloroethylene over Ce–Mn based oxides synthesized by a modified “redox-precipitation route”, Appl. Catal. B: Environ. 172 (2015) 65–72.
[46] T. Chang, Z. Shen, Y. Huang, J. Lu, D. Ren, J. Sun, J. Cao, H. Liu, Post-plasma-catalytic removal of toluene using MnO2–Co3O4 catalysts and their synergistic mechanism, Chem. Eng. J. 348 (2018) 15–25.
[47] Z. Liu, Y. Zhang, S. Jiang, S. Liu, J. Cao, Y. Ai, Enhanced catalytic performance and reduced by-products emission on plasma catalytic oxidation of high-concentration toluene using Mn-Fe/rGO catalysts, J. Environ. Chem. Eng. 10 (2022), 108770.
[48] Z. Wu, D. Zhu, Z. Chen, S. Yao, J. Li, E. Gao, W. Wang, Enhanced energy efficiency and reduced nanoparticle emission on plasma catalytic oxidation of toluene using Au/γ-Al2O3 nanocatalyst, Chem. Eng. J. 427 (2022), 130983.
[49] A.J. Xie, F. Tao, C. Jiang, W.L. Sun, Y.F. Li, L.N. Hu, X. Du, S.P. Luo, C. Yao, A coralliform-structured gamma-MnO2/polyaniline nanocomposite for high-performance supercapacitors, J. Electroanal. Chem. 789 (2017) 29–37.
[50] N. Saheb, S.L, F.S, S. F.H, Kinetics of α- cordierite formation from nano-oxide powders, Ceram. Int. 48 (2022) 3921–23930.
[51] K. Yang, H.W. Shen, Y.Y. Liu, Y. Liu, P.J. Ge, D.Z. Yang, Degradation of tiamulin by a packed bed dielectric barrier plasma combined with TiO2 catalyst, Plasma Sci. Technol. 24 (2022).
[52] S.F. Tang, D.L. Yuan, Y.D. Rao, N. Li, J.B. Qi, T.Z. Cheng, Z.T. Sun, J.M. Gu, H. M. Huang, Persulfate activation in gas phase surface discharge plasma for synergetic removal of antibiotic in water, Chem. Eng. J. 337 (2018) 446–454.
[53] L.A. Rosocha, R.A. Korzekwa, Advanced oxidation and reduction processes in the gas phase using non-thermal plasmas, Los Alamos Natl. Lab NM (1998).
[54] M.F. Mustafa, X. Fu, Y. Liu, Y. Abbas, H. Wang, W. Lu, Volatile organic compounds (VOCs) removal in non-thermal plasma double dielectric barrier discharge reactor, J. Hazard. Mater. 347 (2018) 317–324.
[55] S. Delagrange, L. Pinard, J.-M. Tatibouët, Combination of a non-thermal plasma and a catalyst for toluene removal from air: Manganese based oxide catalysts, Appl. Catal. B: Environ. 68 (2006) 92–98.
[56] M. Šimek, S. Pekárek, V. Prukner, Ozone production using a power modulated surface dielectric barrier discharge in dry synthetic air, Plasma Chem. Plasma Process. 32 (2012) 743–754.
[57] T. Hakoda, H. Goto, A. Shimada, M. Ochi, T. Kojima, Analysis of particles produced by oxidation of dilute xylene in air under electron beam irradiation, Radiat. Phys. Chem. 75 (2006) 375–383.
[58] H.-H. Kim, H. Kobara, A. Ogata, S. Futamura, Comparative assessment of different nonthermal plasma reactors on energy efficiency and aerosol formation from the decomposition of gas-phase benzene, IEEE Trans. Ind. Appl. 41 (2005) 206–214.
[59] T. Yamamoto, B.-L. Jang, Aerosol generation and decomposition of CFC-113 by the ferroelectric plasma reactor, IEEE Trans. Ind. Appl. 35 (1999) 736–742.
[60] H.M. Lee, M.B. Chang, Gas-phase removal of acetaldehyde via packed-bed dielectric barrier discharge reactor, Plasma Chem. Plasma Process. 21 (2001) 329–343.
[61] H. Huang, D. Ye, D.Y. Leung, F. Feng, X. Guan, Byproducts and pathways of toluene destruction via plasma-catalysis, J. Mol. Catal. A: Chem. 336 (2011) 87–93.
[62] S. Liu, D. Mei, L. Wang, X. Tu, Steam reforming of toluene as biomass tar model compound in a gliding arc discharge reactor, Chem. Eng. J. 307 (2017) 793–802.
[63] B. Wang, C. Chi, M. Xu, C. Wang, D. Meng, Plasma-catalytic removal of toluene over CeO2-MnOx catalysts in an atmosphere dielectric barrier discharge, Chem. Eng. J. 322 (2017) 679–692.
[64] Y. Li, Z. Fan, J. Shi, Z. Liu, J. Zhou, W. Shangguan, Modified manganese oxide octahedral molecular sieves M′-OMS-2 (M′= Co, Ce, Cu) as catalysts in post plasma-catalysis for acetaldehyde degradation, Catal. Today 256 (2015) 178–185.
[65] G. Ge, H. Lei, X. Yao, Y. Fang, X. Cheng, Investigation of hybrid plasma-catalytic degradation of toluene over FeOOH/γ-Al2O3 catalysts, J. Environ. Chem. Eng. 11 (2023), 109756.
[66] A.M. Harling, D.J. Glover, J.C. Whitehead, K. Zhang, The role of ozone in the plasma-catalytic destruction of environmental pollutants, Appl. Catal. B: Environ. 90 (2009) 157–161.
[67] G. Zhou, X. He, S. Liu, H. Xie, M. Fu, Phenyl VOCs catalytic combustion on supported CoMn/AC oxide catalyst, J. Ind. Eng. Chem. 21 (2015) 932–941.